

IMAGE RECTIFICATION

Evaluation of Various Projections for Omnidirectional Vision Sensors using the Pixel Density

Christian Scharfenberger, Georg Faerber and Florian Boehm

Institute for Realtime-Computersystems, Technische Universitaet Muenchen, Arcisstrasse 21, 80333 Munich, Germany

Keywords: Omnidirectional vision, Image rectification, Image quality, Calibration, Pixel density.

Abstract: Omnidirectional vision sensors provide a large field of view for numerous technical applications. But the original images of these sensors are distorted, not simply interpretable and not easy to apply for normal image processing routines. So image transformation of original into panoramic images is necessary using various projections like cylindrical, spherical and conical projection, but which projection is best for a specific application?

In this paper, we present a novel method to evaluate different projections regarding their applicability in a specific application using a novel variable, the pixel density. The pixel density allows to determine the resolution of a panoramic image depending on the chosen projection. To achieve the pixel density, first the camera model is determined based on the gathered calibration data. Secondly, a projection matrix is calculated to map each pixel of the original image into the chosen projection area for image transformation. The pixel density is calculated based on this projection matrix in a final step.

Theory is verified and discussed in experiments with simulated and real image data. We also demonstrate that the common cylindrical projection is not always the best projection to rectify images from omnidirectional vision sensors.

1 INTRODUCTION

Many technical tasks require perspective cameras to provide useful information of the surrounding environment. Examples of common application fields are obstacle detection, people tracking and detection. Therefore, cameras are used for driver assistance systems in cars and robotics. There are a couple of reasons to use perspective cameras for different tasks. However, it is desirable in some applications of computational vision to use vision sensors with a large field of view. Teleconferencing, remote surveillance and texture for model acquisition for virtual reality benefit from camera systems providing a large field of view. But normal perspective camera systems are limited in their fields of view. To overcome this limitation, researchers and practitioners developed camera systems containing either rotating (Krishnan and Ahuja, 1996) or multiple cameras (Utsumi et al., 1998). Other, quite effective ways to enhance the field of view are camera systems using wide angle lenses like fisheye lenses or mirrors in conjunction with lenses (Ishiguro, 1998; Daniilidis

and Geyer, 2000; Baker and Nayar, 1999). Omnidirectional vision systems are catadioptric systems and combine a curved mirror with a perspective camera to obtain a large field of view. In the past, several concepts for optical characteristics such as single viewpoint (Baker and Nayar, 1999), (Yamazawa et al., 1993), equi-resolution (Gaspar et al., 2002) and equi-areal (Hicks and Perline, 2002) have been developed to improve omnidirectional camera systems.

1.1 Related Work

Original images of omnidirectional camera systems are distorted, not simply interpretable and not easy applicable to normal image processing routines. Methods and procedures exist which process original images even of uncalibrated omnidirectional vision sensors, but no useful correlation between real object properties like size and width can be found in original images. So there is a need for conventional image processing routines requiring transformed panoramic images as well as calibration information. Yamazawa et al. (Yamazawa et al., 1993) propose methods to

transform warped images into cylindric panoramic images using cylindric coordinates. In (Yamazawa et al., 1998), images of omnidirectional vision sensors (ODVS) are transformed into images as if taken directly with an ordinary camera. These images are suitable for further data analysis, so that conventional image processing routines can be utilised. Gandhi and Trivedi (Gandhi and Trivedi, 2004) use ODVS's with single viewpoints. Knowing the exact parameters of the hyperbolic mirror and the camera, they present a plane transformation method to transform an image to a perspective view looking downwards. Geyer and Daniilidis propose in (Geyer and Daniilidis, 2001) a unifying model for the projective geometry and studied its properties as well as its practical application.

1.2 Motivation

As shown above, various projections are developed to transform original images into unwarped, rectified images for a better use of conventional image processing routines. However, there has been no evaluation in literature that studies and evaluates different projections types to obtain best utilisation of sensor pixels in rectified images. In this paper, we propose a novel value, the pixel density, which characterises the consistence of rectified image pixels with sensor pixels at a certain position. Using the characteristics of the pixel density, the projection for a specific camera system can be chosen for best utilisation of sensor pixels in rectified images. But the pixel density does not predict the distortion of rectified images for a chosen projection. We assume, that the pixel density depends on the chosen projection, the distance between mirror and camera, the field of view of the camera and on the chosen mirror surface. So we conduct experiments on synthesised and real images of ODVS's with different hyperbolic mirrors, different field of views, different distances between mirror and camera as well as various projections. This paper is organised as follows: The camera model and the calibration of omnidirectional vision sensors is introduced in section 2.1 and in section 2.2. We present the rectification methods and the pixel density in section 3 and illustrate our results in section 4. The paper ends with a discussion and conclusion in section 4.2 and section 5.

2 CAMERA CALIBRATION

2.1 Camera Model

We designed ODVS's based on the well illustrated SPOV theorem of Nayar and Baker (Baker and Na-

yar, 1999).

$$\left(z - \frac{c^2}{2}\right) - r^2 \left(\frac{k}{2} - 1\right) = \frac{c^4}{4} \left(\frac{k-2}{k}\right) \quad (1)$$

$$\left(z - \frac{c^2}{2}\right) + r^2 \left(\frac{k}{2} + 1\right) = \left(\frac{2k + c^2}{4}\right) \quad (2)$$

Equation (1) for $k \leq 2$ and equation (2) for $k \geq 2$ dimension ODVS's with single points of view (SPOV), whereas k specifies the mirror surface and c the distance between SPOV and pinhole of the perspective camera. Furthermore, equation (3) fulfils the SPOV theorem for many mirror types like hyperbolic mirrors.

$$\frac{1}{a_h^2} \left(z - \frac{c}{2}\right)^2 - \frac{1}{b_h^2} = 1 \quad \text{with}$$

$$a_h = \frac{c}{2} \sqrt{\frac{k-2}{k}} \quad \text{and} \quad b_h = \frac{c}{2} \sqrt{\frac{2}{k}} \quad (3)$$

In this paper, we use equation (3) to design some real and synthesised mirrors, but we use distances different than c for technical reasons as well as to identify the properties of the pixel density. Using hyperbolic mirrors, the SPOV constraint is only valid for an accurate alignment of mirror and camera. But it is difficult to achieve an exact alignment between mirror and camera, so that the camera system must be calibrated to compensate misalignments and to get a precise relation between world and camera coordinates.

2.2 Calibration

To determine the position of object points, the function $f(\vec{p})$ (4) which describes a relation between \vec{p} in world coordinates x_p, y_p and z_p and the camera coordinates u_p and v_p has to be found (see Figure 1(a)).

$$\vec{P} = \begin{bmatrix} u_p \\ v_p \end{bmatrix} = f(\vec{p}) \quad \text{with} \quad \vec{p} = \lambda \cdot \begin{bmatrix} x_p \\ y_p \\ z_p \end{bmatrix}, \quad \lambda > 0 \quad (4)$$

There exists many methods (Mei and Rives, 2007; Colombo et al., 2007; Baker, S. and Nayar, S., 2001; Micusik and Pajdla, 2004; Scaramuzza et al., 2006a) proposing calibration to determine the function $f(\vec{p})$. We use the calibration method developed by Scaramuzza et al. (Scaramuzza et al., 2006b). All points on a vector \vec{p} in world coordinates (Figure 1(a)) are mapped to the corresponding point P'' on the virtual plane E'' (Figure 1(b)). Scaramuzza et al. propose the

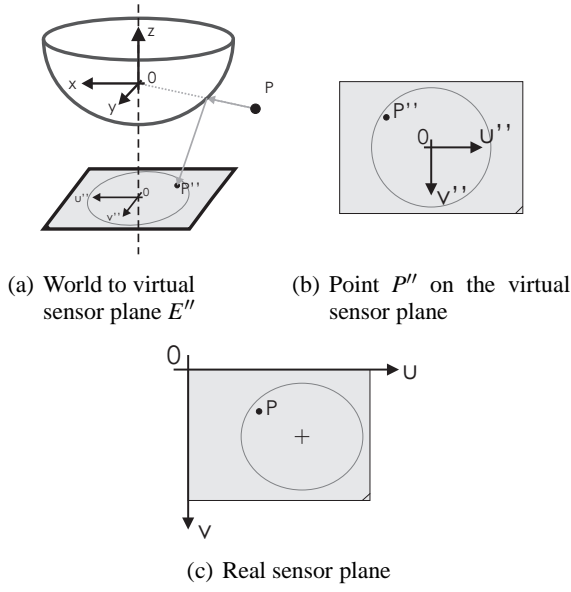


Figure 1: The camera model (a) used in this paper. The world point P is mapped on a virtual sensor plane E'' (b) and the projection transformed to the real sensor plane (c) using affine transformations.

relation between world and virtual sensor plane as

$$\begin{aligned} \vec{p} &= \begin{bmatrix} x_p \\ y_p \\ z_p \end{bmatrix} = \lambda \cdot \begin{bmatrix} u_{p''} \\ v_{p''} \\ f(\rho) \end{bmatrix} \\ &= \begin{bmatrix} x_p \\ y_p \\ a_0 + a_2 \rho^2 + \dots + a_N \rho^N \end{bmatrix} \end{aligned} \quad (5)$$

with $\lambda = 1$ and $\rho = \sqrt{x_p^2 + y_p^2}$. Furthermore, they approximate the component z of $f(\vec{p})$ depending on the curvature as a n -polynomial function. The relation between the real sensor plane and the virtual sensor plane is realised as an affine transformation (see equation 6).

$$\begin{aligned} \vec{p}'' &= \mathbf{A} \cdot \vec{p} + \vec{t} \quad \text{with} \quad \mathbf{A} = \begin{bmatrix} c & d \\ d & 1 \end{bmatrix} \\ \vec{p} &= \begin{bmatrix} u_p \\ v_p \end{bmatrix} \quad \text{and} \quad \vec{t} = \begin{bmatrix} u_{center} \\ v_{center} \end{bmatrix} \end{aligned} \quad (6)$$

The parameters $a_0 \dots a_n$, \mathbf{A} and \vec{t} are the calibration parameters.

3 IMAGE RECTIFICATION

First the projection area in world coordinates based on individual projection parameters like width M , height

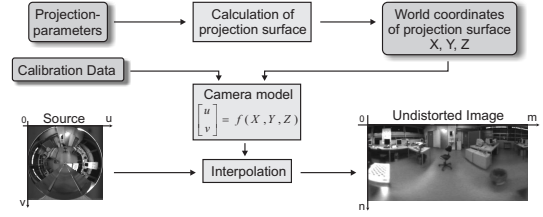


Figure 2: This figure illustrates the rectification of non panoramic images. We calculate the projection area and transform original images to unwrapped image using the gathered calibration data. A bicubic interpolation method is used for interpolation.

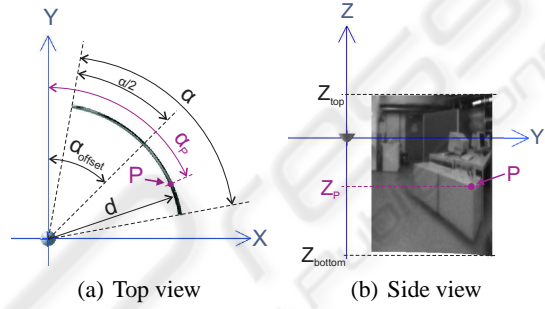


Figure 3: This figure shows the cylindrical projection parameters in top and side view.

N and region of interest (ROI) is determined. Each pixel $[m, n]^T$ of the projection area is stored in a $M \times N \times 3$ dimensional matrix \mathbf{F} containing its world coordinates $\mathbf{X}(m, n)$, $\mathbf{Y}(m, n)$ and $\mathbf{Z}(m, n)$. Furthermore, the sensor coordinates of the projection area are then calculated using the camera model as well as the calibration data and stored in a matrix (LUT). Based on the calibrated camera model, images are rectified using the LUT and a bicubic interpolation method. Figure 2 illustrates this workflow. We also postulate the view of the perspective camera in z -direction for all projections.

3.1 Cylindrical Projection

A common projection is the cylindrical projection. Parameters for the cylindrical projections are distance to the projection area d , rotation width α , rotation offset α_{offset} , and the height of the cylinder given by Z_{top} and Z_{bottom} (see Figure 3(a) and 3(b)). Based on these parameters, first the cylindrical coordinates $(\alpha_p, Z_p)^T$ at position $[m, n]^T$ in the target image with width M and height N are calculated (see equation (7)).

$$\vec{P}_{F, m, n} = \begin{bmatrix} d \\ \alpha_p \\ Z_p \end{bmatrix} = \begin{bmatrix} d \\ (\alpha_{offset} - \frac{\alpha}{2}) + (\frac{\alpha}{M} \cdot m) \\ Z_{top} - \left(\frac{Z_{top} - Z_{bottom}}{N} \cdot n \right) \end{bmatrix} \quad (7)$$

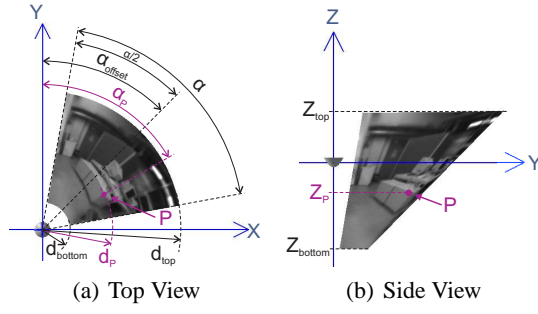


Figure 4: The parameters of conic projection are shown in this figure and define the projecton area.

3.2 Conic Projection

The projection area of the conic projection relates to a cone cut-out. Parameters for the conic projections are distance to the projection area d_{top} and d_{bottom} , rotation width α , rotation offset α_{offset} , and the height of the conic given by Z_{top} and Z_{bottom} (see Figure 4(a) and 4(b)). The cylindrical coordinates $(\alpha_P, Z_P)^T$ of a point P_F at position $[m, n]^T$ in the target image are then determined using equation (8)

$$\vec{P}_{F m, n} = \begin{bmatrix} d \\ \alpha_P \\ Z_P \end{bmatrix} \quad \text{with} \quad \begin{bmatrix} d \\ \alpha_P \\ Z_P \end{bmatrix} = \begin{bmatrix} d_{top} - \left(\frac{d_{top} - d_{bottom}}{N} \cdot n \right) \\ \left(\alpha_{offset} - \frac{\alpha}{2} \right) + \left(\frac{\alpha}{M} \cdot m \right) \\ Z_{top} - \left(\frac{Z_{top} - Z_{bottom}}{N} \cdot n \right) \end{bmatrix} \quad (8)$$

The cartesian coordinates (both for cylindrical and conic projection) of every point are computed using a standard coordinate transformation.

3.3 Spherical Projection

The projection area is a cut-out of a spherical surface. Parameters for the spherical projections are the elevation width β , the elevation offset β_{offset} , the rotation width α and rotation offset α_{offset} (see Figure 5(a) and 5(b)). The spherical coordinates $(\alpha_P, \beta_P)^T$ at position $[m, n]^T$ in the target image are calculated using equation (9) ($r = 1$):

$$\vec{P}_{F m, n} = \begin{bmatrix} r \\ \alpha_P \\ \beta_P \end{bmatrix} = \begin{bmatrix} r \\ \left(\alpha_{offset} - \frac{\alpha}{2} \right) + \left(\frac{\alpha}{M} \cdot m \right) \\ \left(\beta_{offset} + \frac{\beta}{2} \right) - \left(\frac{\beta}{N} \cdot n \right) \end{bmatrix} \quad (9)$$

The spherical coordinates are transformed into cartesian coordinates using the rotation α_P clockwise beginning at the y - axis and the elevation β_P anti-clockwise beginning at the x axis.

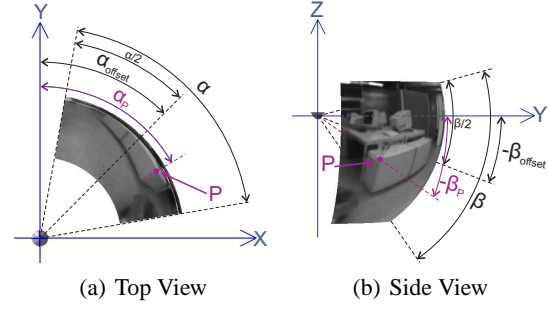


Figure 5: This figure shows the spherical projection parameters in top and side view.

3.4 Pixel Density

To evaluate different projections and to compare different configurations of omnidirectional vision sensors, the position dependent resolution of unwarped images has to be calculated. Therefore, we propose a novel value, the pixel density σ . To determine the pixel density, the distances between pixels in rectified images on the image sensor are determined. Figure 6 demonstrates the basic idea of the pixel density.

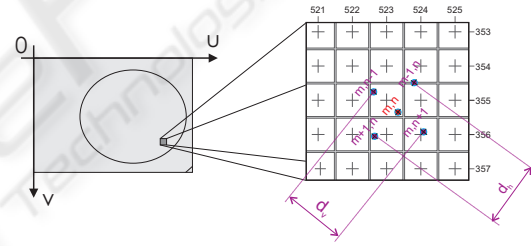


Figure 6: This figure shows the position of pixels in rectified images on the image sensor (left) and its distances (right) on the sensor plane, which are used to calculate the pixel density.

The horizontal pixel density $\sigma_{h(m,n)}$ at position $[m, n]^T$ is calculated using equation (10)

$$\sigma_{h(m,n)} = \frac{1}{2} \cdot d_{h(m,n)} \quad \text{with} \quad (10)$$

$$d_{h(m,n)} = \sqrt{(u_{(m+1,n)} - u_{(m-1,n)})^2 + (v_{(m+1,n)} - v_{(m-1,n)})^2}$$

Analogical, the vertical pixel density $\sigma_{v(m,n)}$ at position $[m, n]^T$ is defined as

$$\sigma_{v(m,n)} = \frac{1}{2} \cdot d_{v(m,n)} \quad \text{with} \quad (11)$$

$$d_{v(m,n)} = \sqrt{(u_{(m,n+1)} - u_{(m,n-1)})^2 + (v_{(m,n+1)} - v_{(m,n-1)})^2}$$

The pixel density $\sigma_{g(m,n)}$ at position $[m, n]^T$ is defined as the geometric mean (see equation (12)) of the horizontal and vertical pixel densities

$$\sigma_{g(m,n)} = \sqrt{\sigma_{h(m,n)} \cdot \sigma_{v(m,n)}} \quad (12)$$

The pixel density σ characterises the consistence of rectified image pixels with sensor pixels, which are used for intensity calculation. Consequently, the pixel density contains the resolution of rectified panoramic images depending on the chosen projection and camera setup. We assume, that best resolution reaches rectified images achieving a pixel density nearly 1. A pixel density less than 1 denotes poor resolution due to less sensor pixels for one pixel in the rectified image, while values larger than 1 denote good resolution but wasting sensor pixels. The pixel density depends on the camera, the chosen projection, the mirror configuration including the curvature as well as the distance between projection center and pinhole.

4 EXPERIMENTAL RESULTS

To evaluate the projections proposed in section 3.1 to 3.3 as well as to analyse the properties of the pixel density, images taken in a synthesised environment and taken in our laboratory are used. The difference between the characteristics of densities of real and synthesised images was less than 0.3 pixels, so that corresponding curves overlap. Therefore and for better understanding, only synthesised images are presented and discussed. For both synthesised and real

Table 1: Overview of the tested parameters.

d (mm)	k	α (degree)
50	5,50	43,00
50	7,55	39,50
50	10,00	36,75
50	7,55	39,50
75	7,55	39,50
100	7,55	39,50
50	7,55	39,50
75	7,55	28,50
100	7,55	22,25

images, we designed various ODVS with different curvatures (k), varying distances (d) between projection center and pinhole as well as diverse field of view (FOV) (α) of the pinhole camera. Secondly, we define a region of interest (ROI) for rectification, unwarped the images using different projections and calculate the pixel density. Table 1 gives an overview of the tested parameters with constant ROI.

4.1 Rotational Symmetric Projections using Synthetic Environments

First, we present the results of our measurements for different distances d between the mirror projection

center and the pinhole (see section 4.1.1). Thereafter, we present the characteristics of the pixel density depending on the chosen projection using constant distances d (see section 4.1.2) and discuss the result in section 4.2. The conic, cylindric and spheric projections are rotationally symmetric, so that the pixel density σ remains constant for all number of columns in the rectified image.

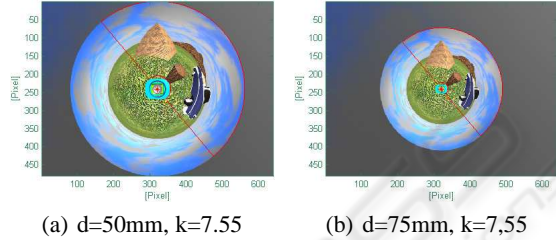


Figure 7: This figure illustrates synthesised images ODVS with constant $k=7.55$, $d=50\text{mm}$ and $d=75\text{mm}$ using the same FOV.

4.1.1 Constant Mirror Type using Varying Distances d as well as FOV

Figure 7 illustrates synthesised images from ODVS with constant mirror type $k=7.55$ and different distances $d=50\text{mm}$ and $d=75\text{mm}$ using the same FOV. Figure 8 shows also the same camera configuration and the same mirror type, but the FOV is adapted to get best utilisation of sensor pixels for image rectification. The marked ROI (red) is used for rectification as well as for calculation the pixel density.

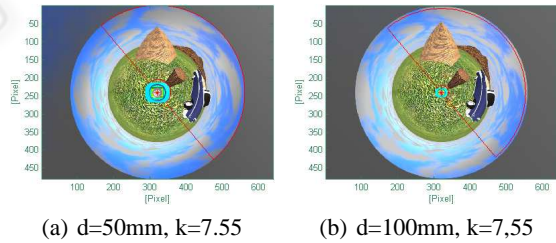


Figure 8: An ODVS with the mirror constant $k=7.55$, different distances and an adapted FOV is used.

Figure 9 demonstrates the result using cylindrical projection, while the characteristics of the pixel density depending on different distances, projections and the chosen field of view (FOV) is presented in figure 10. The charts in the left column (10(a), 10(c), 10(e)) present the results using a constant FOV, while the FOV in (10(b), 10(d), 10(f)) is adapted to get best utilisation of sensor pixels.

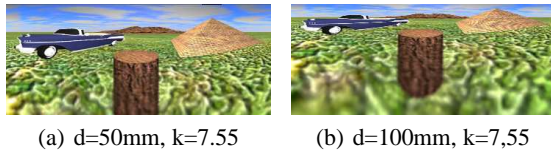
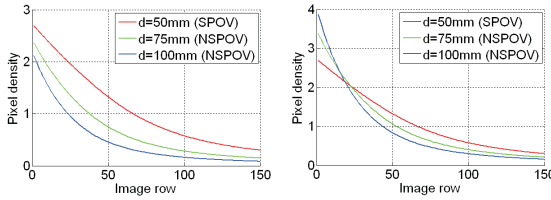
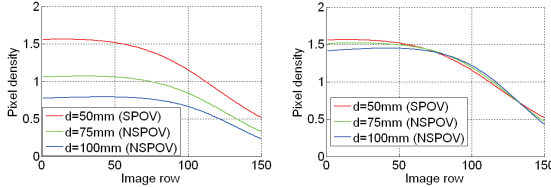


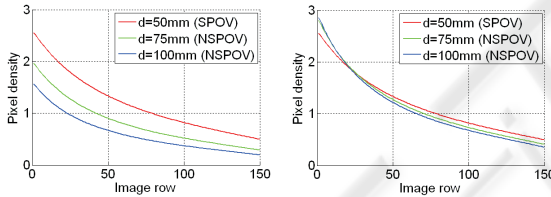
Figure 9: This figure shows unwarped images using cylindrical projection, the same mirror type k but different distances d .



(a) Const. α , $k=7.55$, cyl. (b) Var. α , $k=7.55$, cyl.



(c) Const. α , $k=7.55$, con. (d) Var. α , $k=7.55$, con.



(e) Const. α , $k=7.55$, sph. (f) Var. α , $k=7.55$, sph.

Figure 10: Pixel densities for ODVS's with different distances $d=50\text{mm}$, $d=75\text{mm}$ and $d=100\text{mm}$ as well as fixed FOV's (left) and adapted FOV's (right) using cylindrical, conical and spherical projections.

4.1.2 Results from ODVS with SPOV using Different k 's

To study the influence of the projection, images from omnidirectional vision sensor with single point of view and different mirror types $k = 5, 50$, $k = 7, 55$ and $k = 10, 00$ are generated. Figure 11 shows the original images. We calculated the cylindrical, the conic and the spheric projection and rectified the images using LUT (see section 3).

The rectification result is illustrated in figure 12 for chosen mirror constants. Based on the rectified images, the pixel density σ for each mirror and each projection is determined. The characteristics of the pixel density for the ODVS's with SPOV for different k 's illustrates figure 13.

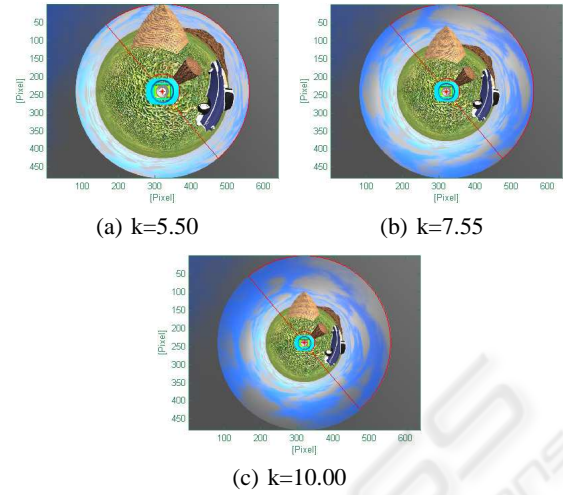


Figure 11: This figure illustrates synthesised images from Single Point of View ODVS with different mirror types. The marked ROI (red) is used for all rectifications.

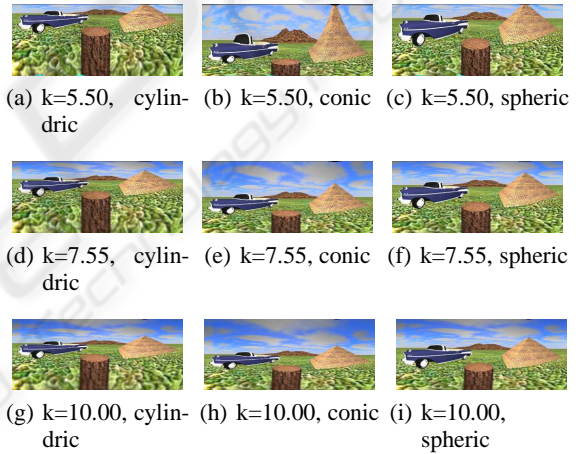


Figure 12: The rectified images for a mirror constant $k = 5.50$, $k = 7.55$ $k = 10.00$ using cylindrical, conic and spheric projection.

4.2 Discussion

Figure 10 and figure 13 present the pixel densities both for synthesised and real images. Measurements show that differences in the pixel density between real and synthesised images were less than 0.3 pixels and not significant. For a better understanding, only the synthesised images are presented and discussed.

The pixel density depends on the ROI, the mirror and camera configuration and the chosen projection. For our studies, we use a ROI including regions under the camera, with short and with large distances to the ODVS. The best resolution reaches a rectified image achieving a pixel density nearly 1. A pixel density less than 1 denotes poor resolution in case of less sensor pixels for one pixel in the rectified image, while a

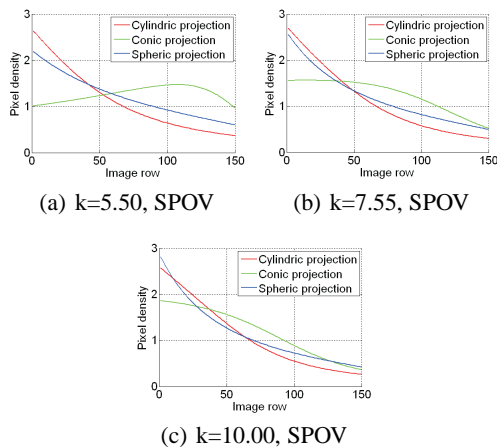


Figure 13: The pixel densities for the different mirrors both for the synthesised and the real rectified images are shown in this diagram.

value larger than 1 denotes good resolution but wasting sensor pixels.

In a first setup, the FOV of the camera remains constant while the distance d between the mirror projection center and camera pinhole increases. As shown in figure 10, the characteristics of pixel density (see 10(a), 10(c), 10(e)) decrease with larger distances d by constant FOV's because less sensor pixels can be used for the light reflected by the mirror.

In a second setup, the FOV is adapted during increasing of the distances d to get the best utilisation of sensor pixels. If the FOV is adapted to the distances to achieve good utilisation of sensor pixels for light reflected by the mirror, pixel density is nearly identical for the same projection type. The small differences as shown in figure (10(b), 10(d), 10(f)) result due to the distance based variance of the vertical FOV. The small differences also result of the increasing vision field of the ODVS by increasing distances d . Figure 9(b) illustrates the larger field of view by the larger distance d compared to 9(a).

In a third setup, we conduct experiments with different projections as well as mirror configurations using cameras with a single point of view. As shown in figure 13, the pixel density with constant sensor resolution varies depending on the chosen projection. The range of the pixel density for cylindrical projection varies in a large range between the upper and the lower image area. The pixel density varies less for the conic projection, therefore the sensor pixel are mapped homogenous to the rectified image. The rectified images using conic projection are the strongest distorted images, but this need not to be a drawback. A good compromise is the spherical projection with less distortion and a nearly homogenous use of sensor pixels in rectified images.

Figure 13 also demonstrates that the common cylindrical projection is not always the best projection for image rectification due to the large range of the pixel density characteristic. Furthermore, the variation of pixel density for cylindrical projection as shown in figure 10 and figure 10(b) is larger than the variation of other projections for different distances between the pinhole of camera and the mirror projection center.

To get best image quality of rectified images, the projection with least variance in the pixel density for different mirrors as well as for various distances between camera pinhole and projection center is recommended. If the distortion of rectified images is not a problem for image processing routines, the conic projection seems to be the best projection due to less variances in the pixel density. Otherwise, the spherical projection can be a good alternative. If only a small region of interest in the projection area is needed for image rectification (for example the area between 50 and 100 pixel (column)), the cylindrical projection can also be a good choice for image rectification. So the pixel density helps to find the projection with optimum use of sensor pixels in rectified images.

Using the LUT as proposed in section 3, online image rectification is possible. Experiments show that only 6.5ms are necessary to transform images with a resolution of $480 \cdot 480$ pixels to unwarped images with a resolution of $540 \cdot 204$ pixels on a 2.2 GHz AMD 64 X2 4200+ processor using bicubic interpolation.

5 CONCLUSIONS AND FUTURE WORK

In this paper, we present methods to rectify and to unwarped distorted images generated by omnidirectional vision sensors (ODVS). Furthermore, we propose a novel value, the pixel density, to evaluate different projections.

The first step is to calibrate the camera providing a relation between world and camera coordinates. Secondly, we present several projections and calculate the projection area to transform original into panoramic images using the calibrated camera model and a LUT containing the world coordinates of every pixel in the transformed region of interest. For our research, we propose a novel value, the pixel density, to evaluate the chosen projection to find best utilisation of sensor pixels in rectified images.

To get best image quality of rectified images, the projection type with least variance in the pixel density both for different mirror types as well as for various distances between the camera pinhole and the projection center is recommend. So the pixel density helps

to find the projection with optimum use of sensor pixels in rectified images.

Further studies of the pixel density and its relation to the projections with different regions of interest (ROI) are necessary. In the next step, the curvature of the pixel density has to be parametrised to find a mathematical relation between the pixel density and the presented projections.

ACKNOWLEDGEMENTS

The authors would like to thank Michelle Karg and the reviewers for their comments which have greatly improved the paper. Support for this research was provided by BMW AG in the framework of CAR@TUM.

REFERENCES

- Baker, S. and Nayar, S. K. (1999). A theory of single-viewpoint catadioptric image formation. *International Journal of Computer Vision*, 35(2):175–196.
- Baker, S. and Nayar, S. (2001). Single viewpoint catadioptric cameras. Monographs in Computer Science.
- Colombo, A., Matteucci, M., and Sorrenti, D. G. (2007). On the calibration of non single viewpoint catadioptric sensors. *Lecture Notes in Computer Science, Springer*, pages 194–205.
- Daniilidis, K. and Geyer, C. (2000). Omnidirectional vision: Theory and algorithms. In Proceedings of the XV International Conference on Pattern Recognition.
- Gandhi, T. and Trivedi, M. M. (2004). Motion analysis for event detection and tracking with a mobile omnidirectional camera. *Multimedia Systems*, 10(2):1432–1882.
- Gaspar, J., Decco, C., Okamoto, J., and Santos-Victor, J. (2002). Constant resolution omnidirectional cameras. In Proceedings of the Third Workshop on Omnidirectional Vision.
- Geyer, C. and Daniilidis, K. (2001). Catadioptric projective geometry. *International Journal of Computervision*, 45(3):223–243.
- Hicks, R. and Perline, R. (2002). Equi-areal catadioptric sensors. In Proceedings of the Third Workshop on Omnidirectional Vision.
- Ishiguro, H. (1998). Development of low-cost compact omnidirectional vision sensors and their applications. In Proceedings of the International Conference on Information Systems, Analysis and Synthesis.
- Krishnan, A. and Ahuja, N. (1996). Panoramic image acquisition. In Proceedings of the IEEE Conference on Computervision and Pattern Recognition.
- Mei, C. and Rives, P. (2007). Single view point omnidirectional camera calibration from planar grids. In Proceedings of the IEEE International Conference on Robotics and Automation.
- Micusik, B. and Pajdla, T. (2004). Para catadioptric camera auto-calibration from epipolar geometry. In Proceedings of the 6th Asian Conference on Computer Vision System.
- Scaramuzza, D., Martinelli, A., and Siegwart, R. (2006a). A flexible technique for accurate omnidirectional omnidirectional camera calibration and structure from motion. In Proceedings of the Fourth IEEE Conference on Computer Vision Systems.
- Scaramuzza, D., Martinelli, A., and Siegwart, R. (2006b). A toolbox for easily calibration omnidirectional cameras. In Proceedings of the IEEE/RSJ International Conference on Intelligent Robots and Systems.
- Utsumi, A., Mori, H., Ohya, J., and Yachida, M. (1998). Multiple-view-based tracking of multiple humans. In Proceedings of the IEEE Conference on Computervision and Pattern Recognition.
- Yamazawa, K., Yagi, Y., and Yachida, M. (1993). Omnidirectional imaging with hyperboloidal projection. In Proceedings of the IEEE/RSJ International Conference on Intelligent Robots and Systems.
- Yamazawa, K., Yagi, Y., and Yachida, M. (1998). Hyperomni vision: Visual navigation with an omnidirectional image sensor. *Systems and Computers in Japan*, 28:36–47.